3536 *Chem. Mater.* **2009,** *21,* 3536–3541
DOI:10.1021/cm803318n

CHEMISTRY OF MATERIALS
Article

Nanoporous $BaTiO_3$ Crystallites

Ru Z. Hou, Paula Ferreira, and Paula M. Vilarinho*

Department of Ceramics and Glass Engineering, CICECO, University of Aveiro, 3810-193 Aveiro, Portugal

Received December 9, 2008. Revised Manuscript Received April 7, 2009

Morphology modification of ferroelectric materials at the nanoscale is an important aspect for further development of ferroelectrics. In this work, the synthesis of nanoporous barium titanate prepared under the assistance of Pluronic PE 10300 block copolymer is reported. Nanopores reside inside the $BaTiO_3$ crystallites that exhibit a specific BET surface area around 70 m^2/g and nanopore volume fraction of 44.7%. X-ray diffraction of nanoporous $BaTiO_3$ indicates an average cubic structure while Raman spectra suggest local structural distortions of the lattice. With Landauer-Bruggeman effective medium approximation (LB-EMA), the dielectric constant (at 1 MHz) of nanoporous $BaTiO_3$ and solid $BaTiO_3$ (excluding all porosity) was estimated as 112 and 706, respectively, implying an effective way to manipulate the dielectric constant of materials by introducing nanopores.

Introduction

Controlling the morphology of ferroelectrics at the nanoscale is bringing a new impetus into the research and development of ferroelectric materials. For example, various one-dimensional structures, such as nanorods, nanowires, and nanotubes, as well as self-assembly of zero-dimensional nanoislands of ferroelectrics have been reported, providing candidates for both fundamental studies and novel applications of ferroelectrics.[1−5] Concomitantly, with artificial polymer opals as templates, inverse opal ferroelectric materials have just emerged as a new kind of three-dimensional photonic crystals with tunable photonic band gap.[6−8] Such materials are composed of periodic ferroelectric building blocks with macropores of several hundred nanometers as intervoids. This idea might be reproduced in a smaller scale with mesopores in the range of 2−50 nm via the approach that is usually used in the synthesis of mesoporous silica or transition metal oxides. Mesoporous $SrTiO_3$ with polycrystalline framework was successfully synthesized with the assistance of a noncommercial block copolymer named KLE3739.[9] However, efforts are still necessary to realize the desired porous structure for complex oxide ferroelectrics with the assistance of common and widely used ionic surfactants or nonionic block copolymers, which are commercially available and of much lower price.

$BaTiO_3$, as a prototype of perovskite ferroelectrics, has been the investigation object from the most classic theories of ferroelectrics to the cutting-edge applications.[10−13] Very recently, the authors reported a facile route to prepare nanosized $BaTiO_3$ single crystals with wormholelike porous structure using cationic surfactant cetyltrimethylammonium chloride (C_{16}TMAC).[14] Because of the disordered nature, thick framework, and pore size of the porous structure, the obtained materials should be better classified as "nanoporous" rather than "mesoporous", the latter usually being characterized by an ordered porosity and very high specific surface area. It should be noticed here that all the reported mesoporous materials prepared with organic soft templates are either amorphous or polycrystalline, which highlights the importance of the porous single crystals. Thus, introducing porosity into $BaTiO_3$ single crystals has not only a significance in the morphology control of ferroelectrics, but also in terms of the exploitation of the synthesis of porous materials which are currently evolving from

*Corresponding author. Fax: 351 234 370204. E-mail: paula.vilarinho@ua.pt.

(1) Urban, J. J.; Yun, W. S.; Gu, Q.; Park, H. *J. Am. Chem. Soc.* **2002**, *124*, 1186.
(2) Mao, Y.; Banerjee, S.; Wong, S. S. *J. Am. Chem. Soc.* **2003**, *125*, 15718.
(3) Morrison, F. D.; Ramsay, L.; Scott, J. F. *J. Phys.: Condens. Matter* **2003**, *15*, L527.
(4) Morrison, F. D.; Luo, Y.; Szafraniak, I.; Nagarajan, V.; Wehrspohn, R. B.; Steinhart, M.; Wendorff, J. H.; Zakharov, N. D.; Mishina, E. D.; Vorotilov, K. A.; Sigov, A. S.; Nakabayashi, S.; Alexe, M.; Ramesh, R.; Scott, J. F. *Rev. Adv. Mater. Sci.* **2003**, *4*, 114.
(5) Alexe, M.; Hesse, D. *J. Mater. Sci.* **2006**, *41*, 1.
(6) Soten, I.; Miguez, H.; Yang, S. M.; Petrov, S.; Coombs, N; Tetreault, N.; Matsuura, N.; Ruda, H. E.; Ozin, G. A. *Adv. Funct. Mater.* **2002**, *12*, 71.
(7) Li, B.; Zhou, J.; Li, Q.; Li, L.; Gui, Z. *J. Am. Ceram. Soc.* **2003**, *86*, 867.
(8) Li, B.; Zhou, J.; Li, L.; Wang, X. J.; Liu, X. H.; Zi, J. *Appl. Phys. Lett.* **2003**, *83*, 4704.
(9) Grosso, D.; Boissière, C.; Smarsly, B.; Brezesinski, T.; Pinna, N.; Albouy, P. A.; Amenitsch, H.; Antonietti, M.; Sanchez, C. *Nat. Mater.* **2004**, *3*, 787.
(10) Cross, L. E.; Nicolson, M. M.; Zlotnicki, B.; Whiddington, R. *Nature* **1950**, *165*, 440.
(11) Cohen, R. E. *Nature* **1992**, *358*, 136.
(12) Junquera, J.; Ghosez, P. *Nature* **2003**, *422*, 506.
(13) Shin, Y. H.; Grinberg, I.; Chen, I. W.; Rappe, A. M. *Nature* **2007**, *449*, 881.
(14) Hou, R. Z.; Ferreira, P.; Vilarinho, P. M. *Microporous Mesoporous Mater.* **2008**, *110*, 392.

Published on Web 07/14/2009

conventional molecular sieve to functional porous crystalline oxides. As a preliminary study, ref 14, did not give a clear description of the porous structure inside $BaTiO_3$ crystallites. And moreover, the effect of nanoporosity on the electric properties has not yet been investigated.

In what concerns the electrical properties, a common thought is that porosity is adverse to both the ferroelectric and dielectric response of the materials. Perfect single crystals or dense ceramics are desired in most cases. But actually, porosity may also have a good impact. A typical example is found in porous pyroelectric films, which exhibit higher pyroelectric figures of merit over their dense counterparts.[15,16] Another example are the porous piezoelectric ceramics known to have high hydrostatic figures of merit and excellent acoustic impedance matching with ambient medium in applications of low-frequency hydrophones and sensors.[17,18] These effects are a direct consequence of the lowering of the dielectric constant of the materials because of the introduction of porosity. By manipulating the volume ratio of porosity, we can adjust the dielectric constant in a wide range. In addition, materials with highly anisotropic dielectric constant can be fabricated with the introduction of aligned pores.[19,20] In the above reports, pores were usually formed by incomplete sintering or using sacrificial pore formers, and thus existed in between the grains. The negative influence of porosity in these applications is the possible degradation of mechanical strengthens of the materials. However, if pores reside inside the grains, this would not be a problem any more.

In this work, nanoporous $BaTiO_3$ crystallites were prepared using a commercially available and inexpensive nonionic block copolymer, Pluronic PE 10300 (BASF) as soft template. A detailed investigation of the obtained nanoporous structures was conducted. The dielectric constant of nanoporous $BaTiO_3$ was evaluated with Landauer-Bruggeman effective medium approximation (LB-EMA), taking the porous material as a diphasic composite. The present results showed an effective reduction of the dielectric constant with the introduction of nanopores into the $BaTiO_3$ crystallites and an effective way to control the dielectric constant.

Experimental Section

Synthesis. 0.015 mol of $TiCl_4$ (Fluka, 99%, 89545) was dissolved in 5 mL of ethanol. The resulting yellow transparent solution was mixed with the block copolymer solution (1 g of Pluronic PE10300 ($EO_{15}PO_{70}EO_{15}$, BASF) dissolved in 30 mL of deionized water) and 0.015 mol $BaCl_2 \cdot 2H_2O$ (Merck, 99%, 1017171000). The solution was kept stirring for 24 h. Then, NaOH (Fluka, 97%, 71692) was added into the solution to increase the pH above 12 and a white gel formed. The gel was refluxed at 363 K for 5 h. The obtained solid products were thoroughly washed and filtered with hot water. Diluted warm aqueous solution of acetic acid (Merck, 99.8%, 1000631011) (17 wt %) was used to diminish the fallout of carbonate and to preliminarily extract part of the block copolymer. Thoroughly washed again with water, the white powders were dried at 333 K in an oven. To remove the block copolymer, the powders at 573 K (BT573), 673 K (BT673), or 873 K (BT873) were calcined for half an hour.

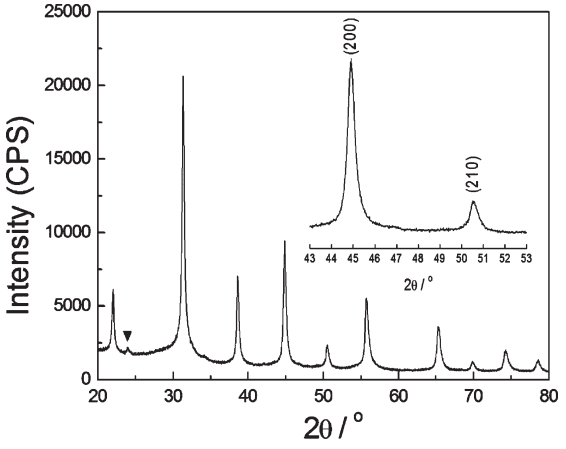

Figure 1. X-ray powder diffraction pattern of the as-synthesized $BaTiO_3$. Diffraction lines from the remnant $BaCO_3$ are marked with "▼". Magnified view of 43−53° region is shown as inset.

Characterization. X-ray diffraction (XRD) data were collected on an X'Pert MPD Philips diffractometer (Cu Kα radiation). The morphology of nanoporous $BaTiO_3$ crystallites was observed with transmission electron microscopy (TEM) and high-resolution transmission electron microscopy (HRTEM) using an Hitachi H9000-NA instrument. Nitrogen adsorption measurements were performed with a Micromeritics Gemini 2375 system at 77 K. Mercury intrusion porosimetry characterization was carried out using PoreSizer 9320 (Micromeritics, Norcross, GA). Raman spectra in the temperature range from 150 to 300 K were acquired with a Bruker RFS 100/S FT Raman spectrometer using a 1064 nm excitation of the Nd/YAG laser. The nanoporous $BaTiO_3$ powders (BT573 and BT873) were isostatically pressed into discs at the pressure of 300 MPa, and metallic gold was then sputtered onto the disk surfaces as electrodes. The dielectric properties were measured with a HP4284A LCR meter.

Results and Discussion

Nanoporous Structure. Figure 1 shows the X-ray powder diffraction pattern of the solid product before calcination. The well-resolved peaks revealed good crystallinity of the obtained $BaTiO_3$ powders, not submitted to any heat treatment. No distinct diffraction feature was found in the small angle range ($0.5° < 2\theta < 5°$). Trace amounts of barium carbonate remained in the powders. The absence of diffraction peak splitting, e.g., (200) and (210) shown in the magnified view of the spectra of Figure 1, points to the presence of a cubic structure for these nanoporous $BaTiO_3$ powders at room temperature. The following calcination caused no significant changes in the XRD spectra except for a slight shift

(15) Seifert, A.; Muralt, P.; Setter, N. *Appl. Phys. Lett.* **1998**, *72*, 2409.
(16) Suyal, G.; Seifert, A.; Setter, N. *Appl. Phys. Lett.* **2002**, *81*, 1059.
(17) Hikita, K.; Yamada, K.; Nishioka, M.; Ono, M. *Ferroelectrics* **1983**, *49*, 265.
(18) Bowen, C. R.; Perry, A.; Lewis, A. C. F.; Kara, H. *J. Eur. Ceram. Soc.* **2004**, *24*, 541.
(19) Gong, X.; She, W. H.; Hoppenjans, E. E.; Wing, Z. N.; Geyer, R. G.; Halloran, J. W.; Chappell, W. J. *IEEE Trans. Microwave Theory Tech.* **2005**, *53*, 3638.
(20) Wing, Z. N.; Wang, B.; Halloran, J. W. *J. Am. Ceram. Soc.* **2006**, *89*, 3696.

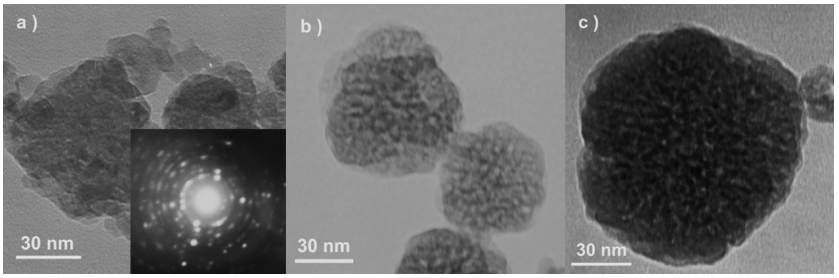

Figure 2. TEM micrographs of (a) as-synthesized $BaTiO_3$ crystallites and the selected area electron diffraction (SAED), (b) nanoporous $BaTiO_3$ calcined at 573 K and (c) at 673 K.

of the XRD peak position to higher diffraction angles was observed. The observed shrinkage of the lattice is attributed to the diminishment of lattice defects, such as hydroxyl groups, that occurs with the heat treatment.

According to the TEM analysis of as-synthesized powders (Figure 2a), the size of $BaTiO_3$ crystallites varied from several to tens of nanometers. TEM microstructures of calcined samples, intentionally taken on isolated crystallites with relatively large size, are shown in images b and c in Figure 2. For both BT573 and BT673 samples, disordered nanoporous structures were observed. To confirm the single-crystalline nature of the framework, we conducted HRTEM studies; a typical image is shown in Figure 3a. For the whole particle, the fringes are in the same direction only with interruptions caused by the pores. The fast Fourier transform (FFT) image is given as inset. Based on the fast Fourier transform (FFT)-filtered image shown in Figure 3b, the nanoporous structure inside $BaTiO_3$ crystallite is portrayed. Wormholelike pores (represented by the shadow where fringes break) are interspersed inside the single crystallite with a thick framework. They are interconnected and wind to the surface of the crystallite in a completely irregular way. The shape of the pores is also irregular and cannot be simply described as cylindrical, nor ink-bottled, nor slit shape. Such porous structures can not be compared with those usually observed in mesoporous silica, but a similar case is found in mesoporous single-crystalline particles of niobium−tantalum mixed oxide.[21]

The absence of pore ordering suggests that there was no strong interaction between the hydrophilic part of the block copolymer and the oxo-titanium during nucleation and growth of $BaTiO_3$ crystallites in the solution. When nonionic block copolymer is used as template, the cooperative assembly of inorganic and organic components in the solution is attributed to hydrogen bonding pathway $(S^0H^+)(X^-I^+)$ in an acid condition.[22] Although the precursor solution of the present process was highly acidic because of the generation of HCl from the reaction between $TiCl_4$ and ethanol, the following addition of NaOH by the requirement of basic conditions to form $BaTiO_3$ crystals contradicts the hydrogen bonding

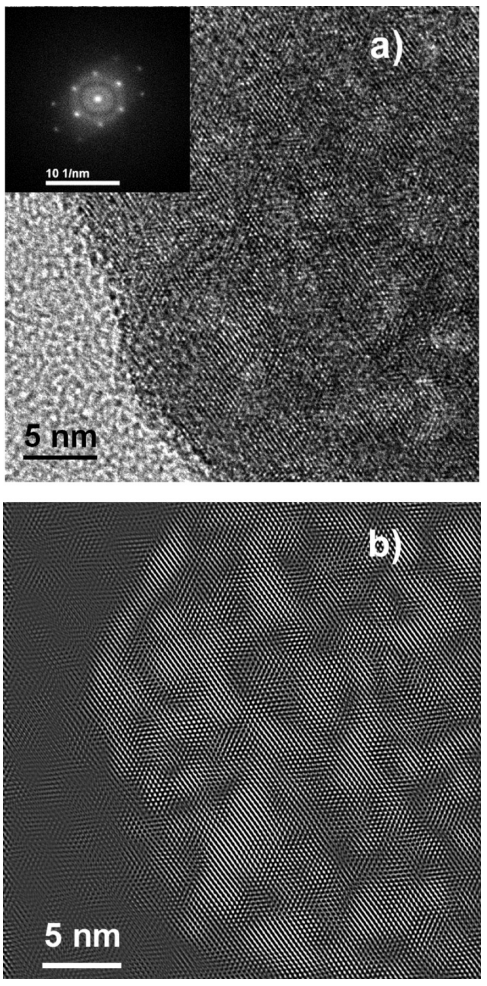

Figure 3. (a) HRTEM image of a single nanoporous $BaTiO_3$ crystal (BT573) showing the lattice broken by pores. Inset is the FFT image. (b) Corresponding FFT-filtered image illustrating the disordered porous structure inside the crystal.

pathway, resulting in a disordered porous structure. It is well-known that ordered mesoporous structures can be easily achieved for amorphous silica via soft chemistry.[23,24] With careful calcination, or assembly of nanocrystals around the template, or replication from mesoporous template, ordered mesoporous structures

(21) Lee, B.; Yamashita, T.; Lu, D.; Kondo, J. N.; Domen, K. *Chem. Mater.* **2002**, *14*, 867.
(22) Zhao, D. Y.; Huo, Q. S.; Feng, J. L.; Chmelka, B. F.; Stucky, G. D. *J. Am. Chem. Soc.* **1998**, *120*, 6024.
(23) Kresge, C. T.; Leonowicz, M. E.; Roth, W. J.; Vartuli, J. C.; Beck, J. S. *Nature* **1992**, *359*, 710.
(24) Beck, J. S.; Vartuli, J. C.; Roth, W. J.; Leonowicz, M. E.; Kresge, C. T.; Schmitt, K. D.; Chu, C. T-W.; Olson, D. H.; Sheppard, E. W.; McCullen, S. B.; Higgins, J. B.; Schlenker, J. L. *J. Am. Chem. Soc.* **1992**, *114*, 10834.

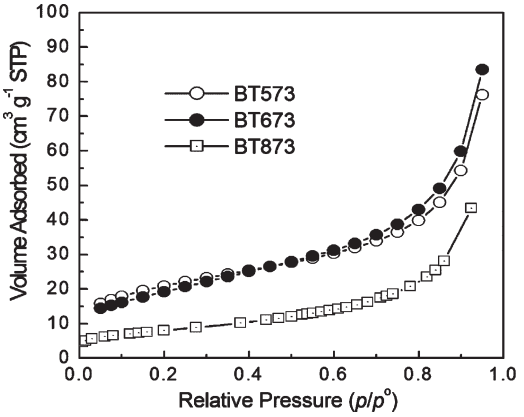

Figure 4. Nitrogen adsorption isotherms of nanoporous $BaTiO_3$ calcined at 573, 673, and 873 K.

can also be attained for functional metal oxides.[9,25−28] However, to the best knowledge of the present authors, there is no successful synthesis of oxide single crystal with ordered mesoporous structure using soft templates.

Figure 4 shows the nitrogen adsorption isotherms of the nanoporous $BaTiO_3$ calcined at different temperatures. The specific Brunauer−Emmett−Teller (BET) surface areas were 72.6 m^2/g and 69.1 m^2/g for BT573 and BT673, respectively. These values are higher than the surface area of 50.2 m^2/g of porous $BaTiO_3$ prepared with cationic surfactant $C_{16}TMAC$.[14] According to this, there was no obvious porosity degradation when the calcination temperature was up to 673 K. Calcination at further higher temperature led to an obvious decrease in the BET surface area (43.6 m^2/g for BT873), most likely due to the closure and collapse of the pores upon heating. Mercury intrusion porosimetry was employed to characterize the BT573 powders with a maximum pressure of 30000 pounds per square inch. The accessible pore size limit is 6 nm for the current mercury intrusion. Thus, the intruded mercury was supposed to completely fill in the intervoids among the particles but not the nanopores inside $BaTiO_3$ crystallites. On this basis, an apparent density of 3.25 g/cm^3, defined as density of the material including closed and inaccessible pores, was attained. This apparent density reflects a nanopore volume fraction of 44.7%, much higher than that of porous $BaTiO_3$ (27%) prepared with $C_{16}TMAC$.[14]

Structure Features. It is well-known that the stability of the ferroelectric phase is closely related with factors such as grain size, stress, dopant, defects, surface area, among other aspects. The high specific surface area caused by the nanoporosity might influence the lattice structure and crystallographic phases of $BaTiO_3$ which possesses a tetragonal structure at room temperature in single crystals or bulk ceramics with coarse grains. $BaTiO_3$ undergoes three phase transitions as the temperature increases:

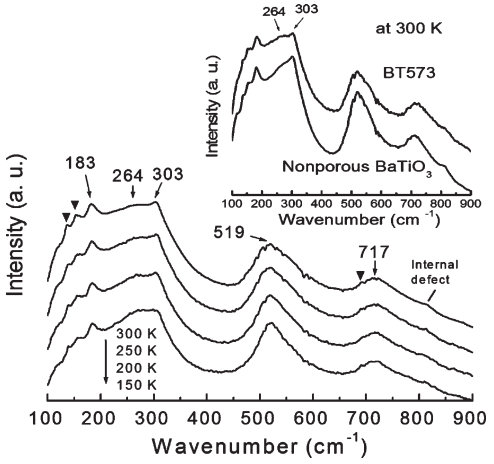

Figure 5. Raman spectra of nanoporous $BaTiO_3$ (BT573) measured at various temperatures. A comparison between the Raman spectra of BT573 and nonporous $BaTiO_3$ at 300 K is shown as inset. Peaks of $BaCO_3$ are marked with "▼".

from rhombohedral to orthorhombic at 183 K, to tetragonal at 278 K and to the cubic phase at 393 K.[29] Among them, the tetragonal to cubic phase transition in bulk $BaTiO_3$ is particularly relevant because it is responsible for the abrupt vanishing of spontaneous polarization. Raman spectroscopy is sensitive to the variation of the crystal structure, and thus was used to study the structural details of nanoporous $BaTiO_3$ in this work. The Raman spectra collected from 150 to 300 K with 50 K intervals are depicted in Figure 5.

Mainly, the obtained spectra are characterized with five bonds situated at 183, 264, 303, 519, and 717 cm^{-1}. Bands at 303 and 717 cm^{-1}, which would not be present in the cubic phase, have been commonly used as the indication of the $BaTiO_3$ polar phase.[30−32] They are clearly distinguished in Figure 5. The broadband around 264 cm^{-1} is assigned to an $A_1(TO)$ mode which comes from the splitting of triply degenerated soft mode $F_{1u}(TO)$ in the cubic phase.[33] A slight softening and intensity decrease of the 264 cm^{-1} band was observed as the temperature increased from 150 to 300 K. Signals at 135, 153, and 692 cm^{-1} are from residual $BaCO_3$, whereas the one at 814 cm^{-1} was judged to be due to internal defects.[34] Despite the unsplit XRD lines, the Raman results strongly suggest the existence of local structural distortions away from cubic structure. According to the most recent works on the comprehension about size effects in perovskite ferroelectrics, there is no particular critical size at which the spontaneous polarization vanishes but instead the gradual loss of the coherency of the structural

(25) Shibata, H.; Ogura, T.; Mukai, T.; Ohkubo, T.; Sakai, H.; Abe, M. *J. Am. Chem. Soc.* **2005**, *127*, 16396.
(26) Kirsch, B. L.; Richman, E. K.; Riley, A. E.; Tolbert, S. H. *J. Phys. Chem. B* **2004**, *108*, 12698.
(27) Ba, J.; Polleux, J.; Antonietti, M.; Niederberger, M. *Adv. Mater.* **2005**, *17*, 2509.
(28) Luo, J.; Wang, Y.; Xiong, H.; Xia, Y. *Chem. Mater.* **2007**, *19*, 4791.
(29) Haertling, G. H. *J. Am. Ceram. Soc.* **1999**, *82*, 797.
(30) Wang, X.; Deng, X.; Wen, H.; Li, L. *Appl. Phys. Lett.* **2006**, *89*, 162902.
(31) Buscaglia, V.; Buscaglia, M. T.; Viviani, M.; Mitoseriu, L.; Nanni, P.; Trefiletti, V.; Piaggio, P.; Gregora, I.; Ostapchuk, T.; Pokorný, J.; Petzelt, J. *J. Eur. Ceram. Soc.* **2006**, *26*, 2889.
(32) Ostapchuk, T.; Pokorný, J.; Pashkin, A.; Petzelt, J.; Železný, V.; Rafaja, D.; Drbohlav, I. *J. Eur. Ceram. Soc.* **2005**, *25*, 3063.
(33) Luspin, Y.; Servoin, J. L.; Gervais, F. *J. Phys. C: Solid State Phys.* **1980**, *13*, 3761.
(34) Shiratori, Y.; Pithan, C.; Dornseiffer, J.; Waser, R. *J. Raman Spectrosc.* **2007**, *38*, 1288.

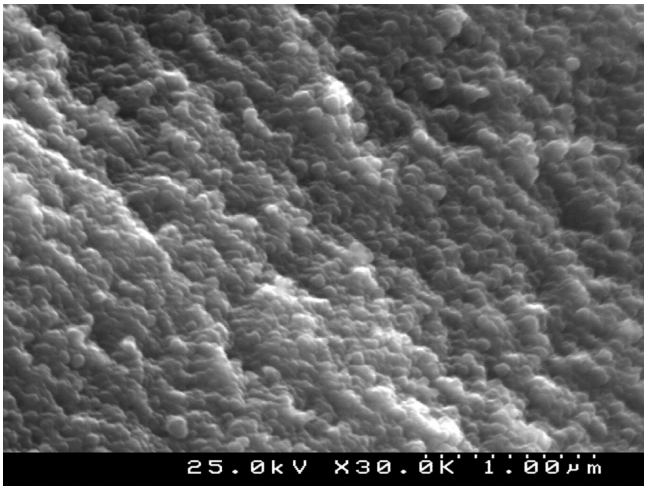

Figure 6. SEM image of the fracture surface of an isostatic-pressed nanoporous $BaTiO_3$ disk.

distortion leads to the average cubic structure as the crystal dimension decreases.[35−37] The present nanoporous $BaTiO_3$ should also be included in this situation in which Ti atoms displace from the equilibrium positions forming local polar ordering but without long-range correlations. A comparison is made between the 300 K Raman spectra of BT573 and nonporous $BaTiO_3$ nanocrystallites (inset of Figure 5). The nonporous $BaTiO_3$ crystallites were prepared using the same process as nanoporous $BaTiO_3$, except that there was no block copolymer in the initial solution. A slight decrease in the intensity of the 303 cm^{-1} band and a broadening of the 264 cm^{-1} band are found for BT573 when compared to nonporous nanocrystallites. This difference should come from the intensified atoms position disorder and structure incoherence due to the high surface to volume ratio in nanoporous $BaTiO_3$ crystals.

Evaluation of the Dielectric Constant of Nanoporous $BaTiO_3$. Because a high-temperature sintering would greatly change the porous structure, the dielectric characterization of the nanoporous $BaTiO_3$ crystallites was conducted on isostatic-pressed pellets. The facture SEM micrograph of a BT573 isostatic-pressed pellet is shown in Figure 6. The total porosity of the pressed disk is composed of (i) the porosity among particles, called intergranular porosity, that can be observed by SEM, and (ii) the nanoporosity inside each crystallite. The average bulk density (2.27 g/cm^3) of BT573 discs, determined by weight and size measurements, indicates a 61.4% total volume fraction of pores. Taking the mercury intrusion porosimetry data into account, the volume fractions of intergranular voids, nanopores and solid $BaTiO_3$ of the pressed pellet were determined as 30.2, 31.2, and 38.6%, respectively. The two components of porosity were almost equivalent in the as-pressed samples.

Porous dielectrics can be considered as a composite of two phases: a solid one and the air. Various models have been used for the evaluation of the dielectric constant of a diphasic composite.[20,38−41] Thus, the effective dielectric constant of nanoporous $BaTiO_3$ and the real dielectric constant of the solid $BaTiO_3$ can be estimated with the dielectric mixture model using the data obtained from the dielectric measurements of isostatic-pressed discs. Obviously, the simplest parallel and perpendicular models are not suitable for describing the nanoporous crystallites. Maxwel-Garnett (MG) model[38] and Landauer-Bruggeman effective medium approximation (LB-EMA)[39,40] are commonly accepted laws to treat diphasic composite systems in which the second phase is randomly distributed in the matrix. LB-EMA is more general and valid for arbitrary inclusion concentration, whereas MG is suitable for dilute inclusions without percolation phenomenon.[41,42] Considering the high pore volume fraction and pore connection in the nanoporous sample, LB-EMA is used in this work rather than MG for evaluation of the dielectric response. The description in terms of mathematical expression of LB-EMA is

$$v\frac{\varepsilon_1-\varepsilon_{\text{eff}}}{\varepsilon_1+2\varepsilon_{\text{eff}}}+(1-v)\frac{\varepsilon_2-\varepsilon_{\text{eff}}}{\varepsilon_2+2\varepsilon_{\text{eff}}}=0 \qquad (1)$$

where v denotes the volume fraction of inclusion, and ε_{eff}, ε_1, and ε_2 stand for the dielectric constant of the composite, inclusion, and matrix, respectively. Here, air is the inclusion and thus $\varepsilon_1 = 1$.

The measured effective dielectric constant of BT573 pressed discs decreases from ~210 (at 10 kHz) to ~60 (at 1 MHz) as function of the frequency (Figure 7a). The values of BT873 increase to around 500, indicating a degradation of the sample porosity. This is consistent with the nitrogen adsorption result. Excluding the effects of intergranular voids, LB-EMA estimation gives that the dielectric constant of nanoporous $BaTiO_3$ decreases from ~375 to ~110 as frequency increases from 10 kHz to 1 MHz. When excluding all the porosity, the calculated dielectric constant of solid $BaTiO_3$ is in the range from ~2530 (at 10 kHz) to ~700 (at 1 MHz). The large frequency dependence of the dielectric constant implies a contribution from extrinsic mechanisms at low frequency, such as interfacial polarization or space charges. The estimated values of solid $BaTiO_3$ near 1 MHz are reasonable and similar to the reported data for nanograined $BaTiO_3$ ceramics or films.[31,43] These results suggest that the dielectric constant can be drastically lowered with the introduction of nanoporosity. Thus, the manipulation of the dielectric constant in a wide range

(35) Smith, M. B.; Page, K.; Siegrist, T.; Redmond, P. L.; Walter, E. C.; Seshadri, R.; Brus, L. E.; Steigerwald, M. L. *J. Am. Chem. Soc.* **2008**, *130*, 6955.
(36) Petkov, V.; Buscaglia, V.; Buscaglia, M. T.; Zhao, Z.; Ren, Y. *Phys. Rev. B* **2008**, *78*, 054107.
(37) Petkov, V.; Gateshki, M.; Niederberger, M.; Ren, Y. *Chem. Mater.* **2006**, *18*, 814.
(38) Maxwell-Garnett, J. C. *Philos. Trans. R. Soc. London A* **1904**, *203*, 385.
(39) Bruggeman, D. A. G. *Ann. Phys.* **1935**, *24*, 636.
(40) Landauer, R. *J. Appl. Phys.* **1952**, *23*, 779.
(41) Hudák, O.; Rychetský, I.; Petzelt, J. *Ferroelectrics* **1998**, *208*, 429.
(42) Kärkkäinen, K.; Sihvola, A.; Nikoskinen, K. *IEEE Trans. Geosci. Remote Sensing* **2001**, *39*, 1013.
(43) Ihlefeld, J. F.; Borland, W. J.; Maria, J. P. *Adv. Funct. Mater.* **2007**, *17*, 1199.

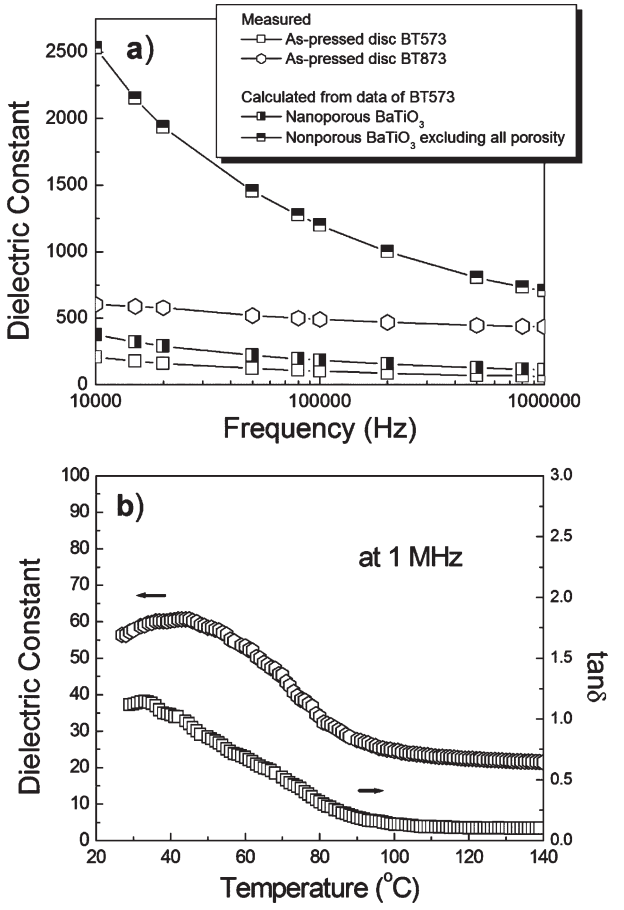

Figure 7. (a) Measured dielectric constant of isostatic-pressed discs (BT573 and BT873) as a function of the frequency; calculated dielectric constant of nanoporous $BaTiO_3$ crystallites and solid $BaTiO_3$ without any porosity using LB-EMA.[39,40] (b) Temperature dependence of the dielectric constant and tanδ of BT573 discs at 1 MHz.

is possible by changing the volume fraction of nanopores. The way to modify the volume fraction of nanopores is not only by varying the initial block copolymer content but also by changing the post heat treatment.

The temperature dependence of the dielectric constant, ε_r, and losses, tan δ (at 1 MHz), of BT573 pressed discs are depicted in Figure 7b. As the temperature decreases, the dielectric constant and the losses increase and no evidence of ferroelectric phase transition around 120 °C is observed, proving the absence of long-range polarization and confirming the XRD analysis. Instead, there is a plateau above room temperature in both the plots. Although not sufficiently studied, this behavior seems not to be due to extrinsic polarizations because the dielectric constant and tan δ decrease to a lower level with increasing temperature. Instead it may be related to the response of the short-range polarization, which is derived from local structural distortions as indicated by Raman spectrum and fades out as temperature increases. Local characterization by scanning probe microscopy is now underway to further clarify the electric response of these nanoporous $BaTiO_3$ powders.

Summary

Nanoporous $BaTiO_3$ crystallites were prepared with the assistance of nonionic block copolymer Pluronic PE 10300 via a simple route. After the removal of the template, interconnected pores were left inside the $BaTiO_3$ crystallites. The product showed specific BET surface areas around 70 m^2/g and nanopore volume fraction of 44.7%, which are higher than those of reported porous $BaTiO_3$ prepared with cationic surfactant C_{16}TMAC.[14] Nanoporous $BaTiO_3$ possess an average cubic structure but with local structural distortions. Dielectric constant of $BaTiO_3$ was drastically decreased with the introduction of nanopores implying an effective way to manipulate the dielectric constant especially where low dielectric constant is desired to achieve high figures of merit in pyroelectric and piezoelectric applications. This work indicates that besides the particle size, nanoporosity influences the structure and physical properties of ferroelectrics. The authors hope that these findings will open new ways for a better comprehension of the effects of surface area, surface curvature, and surface charges on ferroelectrics at the nanoscale.

Acknowledgment. The authors are thankful to Dr. Marc Willinger for HRTEM characterizations. Dr. Mariana Sardo and Prof. Paulo Claro are acknowledged for the help with Raman spectroscopy. The authors are grateful to BASF for providing the block copolymer. This work was funded by FCT under Grant SFRH/BPD/26711/2006, FEDER and European Network of Excellence FAME under Contract FP6-500159-1.